Electronic Supplementary Material (ESI) for Dalton Transactions

Supporting Information for

Network Formation and Photoluminescence in Copper(I) Halide Complexes with Substituted Piperazine Ligands

Jason P. Safko,[a] Jacob E. Kuperstock,[a] Shannon M. McCullough,[a] Andrew M. Noviello,[a] Xiaobo Li,[b] James P. Killarney,[b] Caitlin Murphy,[b] Howard H. Patterson,[b] Craig A. Bayse,[c] and Robert D. Pike[a]*

[a]*Department of Chemistry, College of William and Mary, Williamsburg, VA 23187-8795.*

[b]*Department of Chemistry and Biochemistry, Old Dominion University, Norfolk, VA 23529.*

[c]*Department of Chemistry, University of Maine, Orono, ME 04469-5706.*

Email: rdpike@wm.edu

Contents

X-ray Powder Patterns……3

Thermogravimetric Traces……13

Luminescence Spectra……...18

Plots of the cluster-based molecular orbitals of $(CuI)_2(NMe_3)_2$ (**Y**)……..23

Figure S1. Experimental and calculated powder diffractograms of $(CuBr)_4(\mathbf{1})_2$.

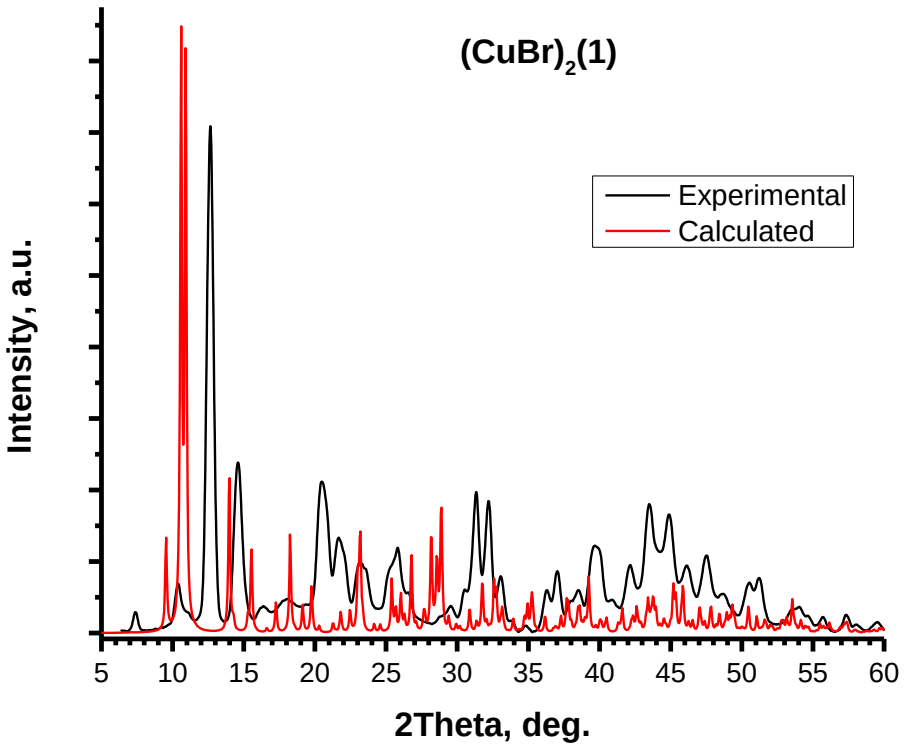

Figure S2. Experimental and calculated powder diffractograms of CuI + **1** products.

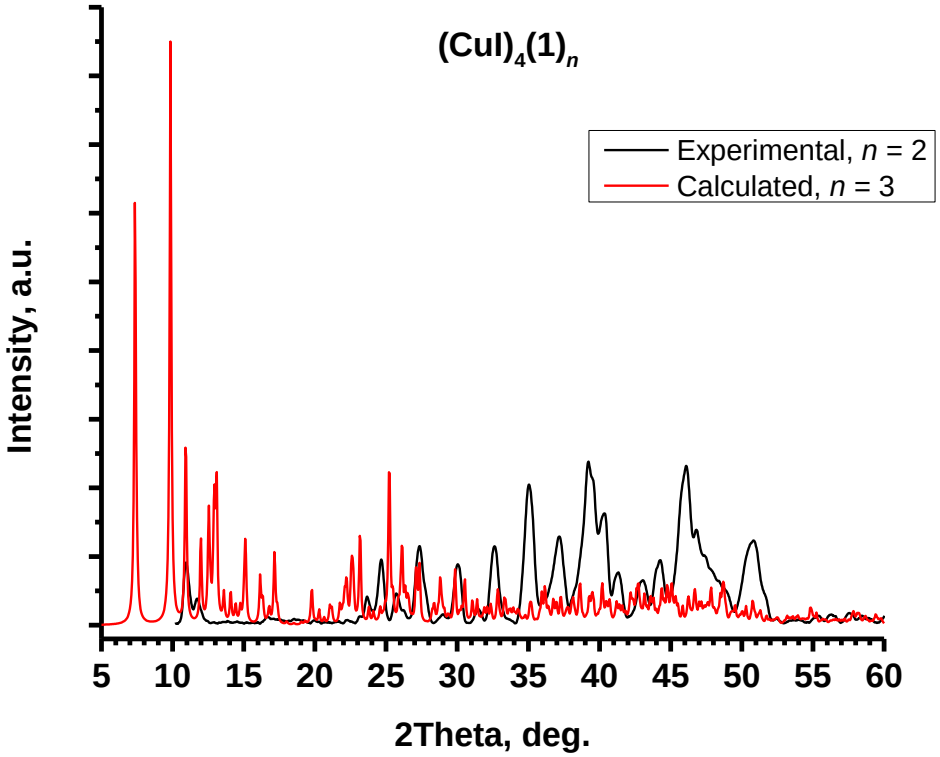

Figure S3. Experimental and calculated powder diffractograms of $(CuBr)_4(\mathbf{2})_2$.

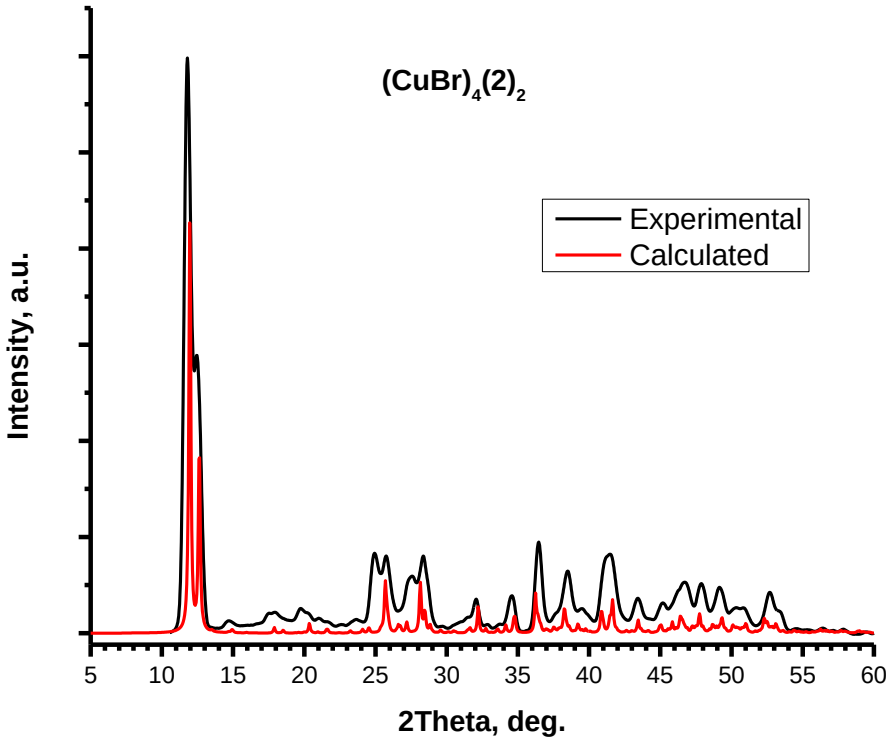

Figure S4. Experimental and calculated powder diffractograms of $(CuI)_4(\mathbf{2})_2$.

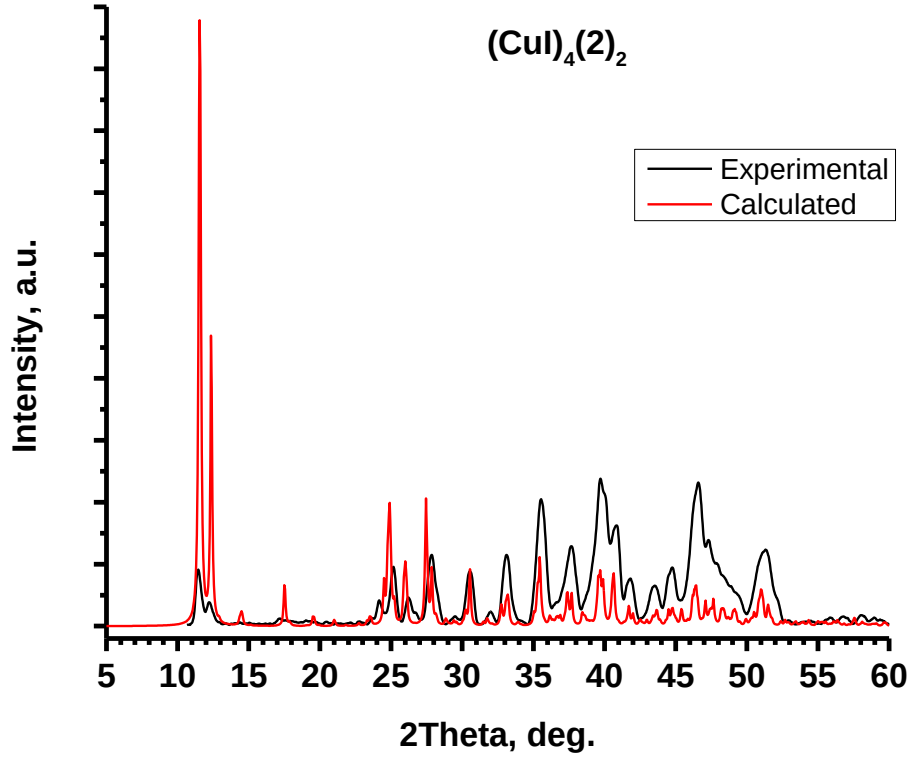

Figure S5. Experimental and calculated powder diffractograms of $(CuI)_2$(**3**).

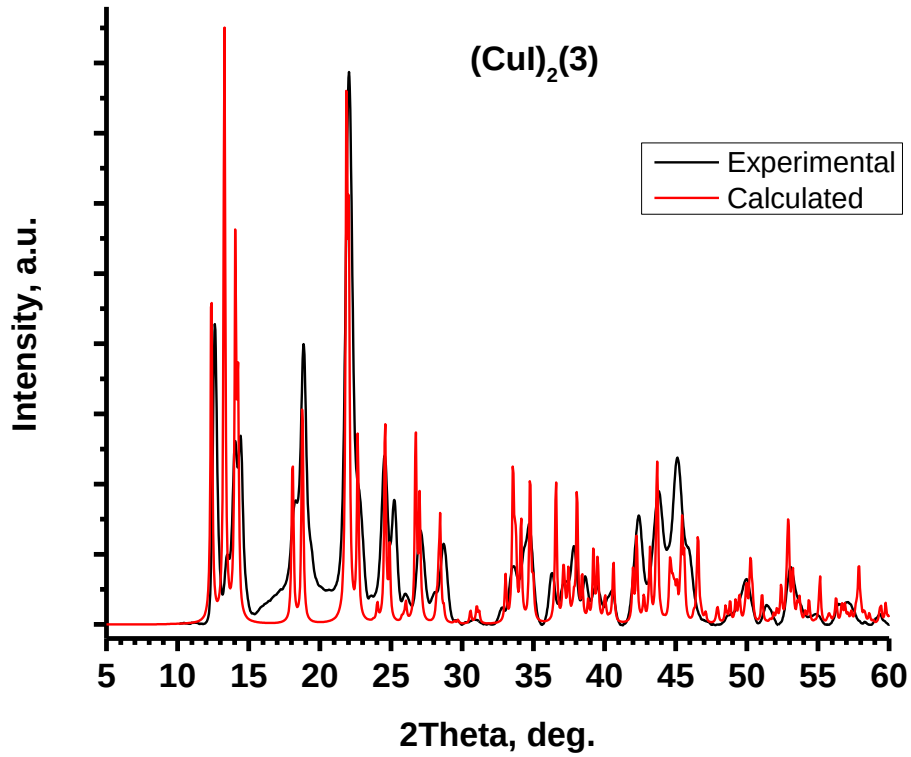

Figure S6. Experimental and calculated powder diffractograms of $(CuI)_2$(**4**).

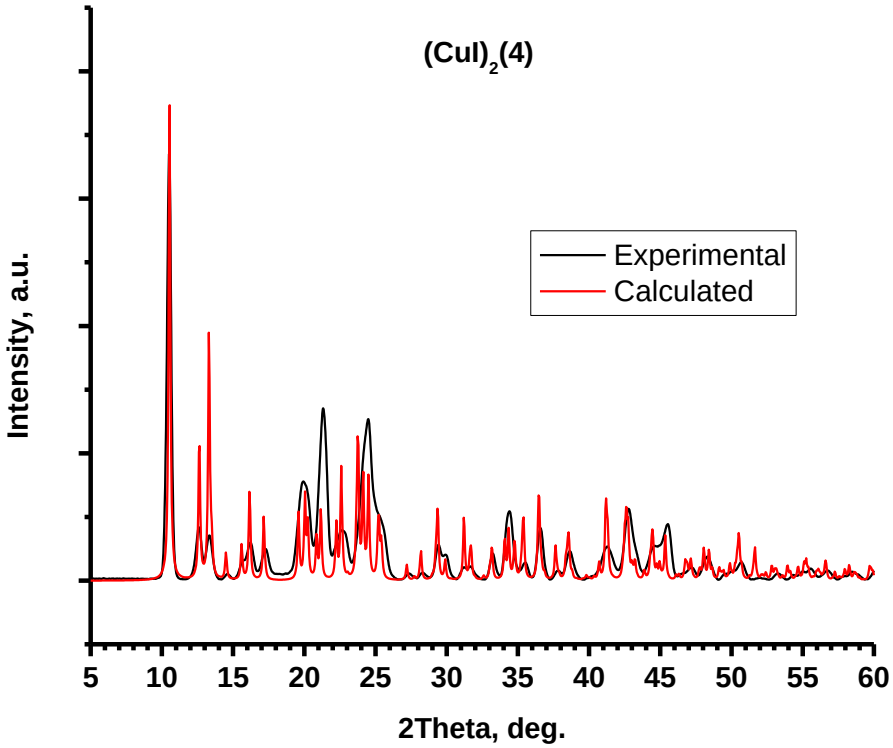

Figure S7. Experimental and calculated powder diffractograms of $(CuI)_2$(**5**).

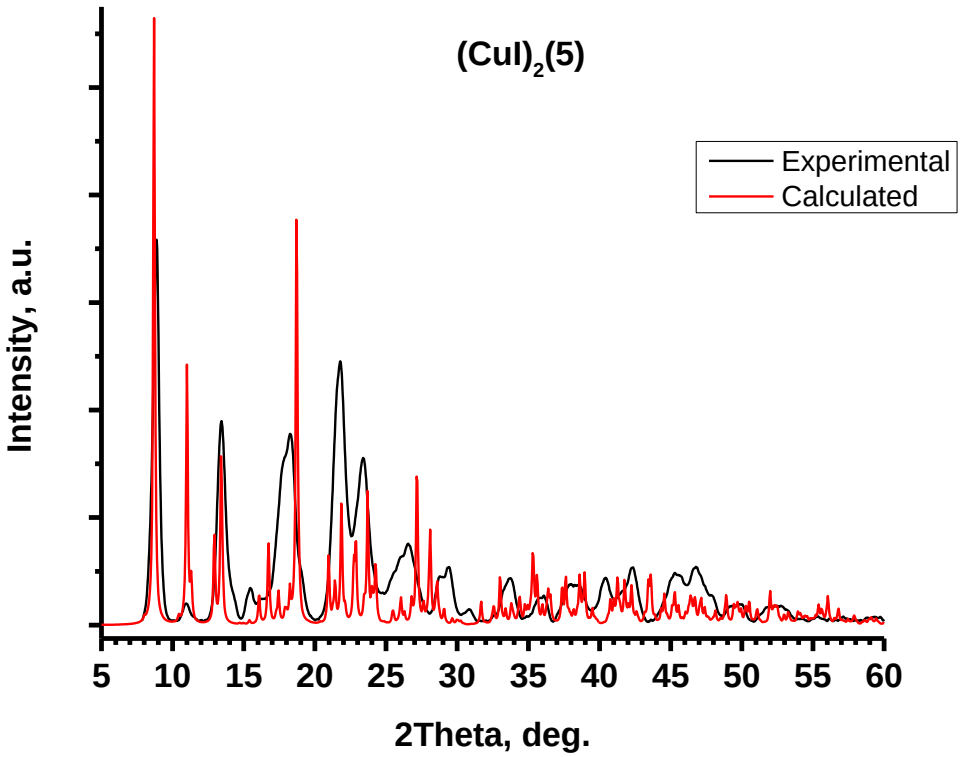

Figure S8. Experimental and calculated powder diffractograms of $(CuI)_4(\mathbf{6})_4$.

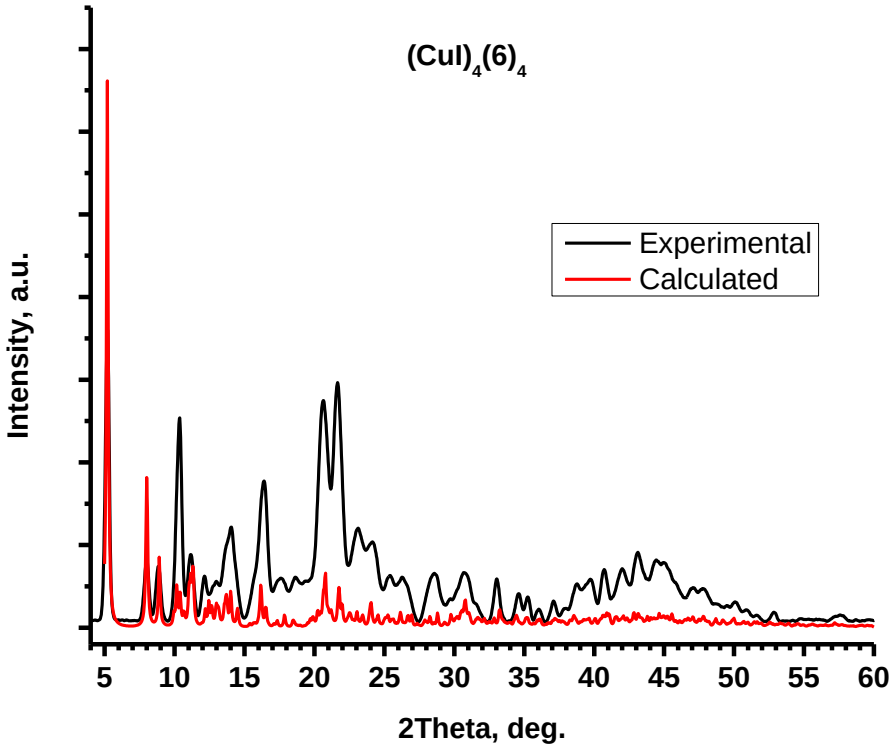

Figure S9. Experimental and calculated powder diffractograms of $(CuI)_2$(**7**).

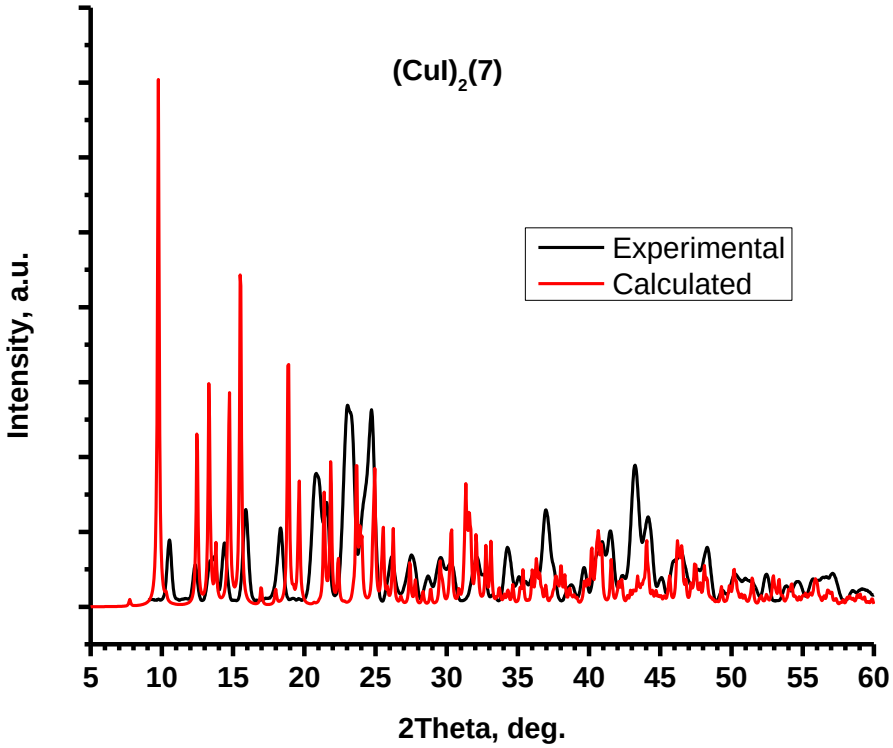

Figure S10. Experimental and calculated powder diffractograms of $(CuI)_2(\mathbf{8})_2$.

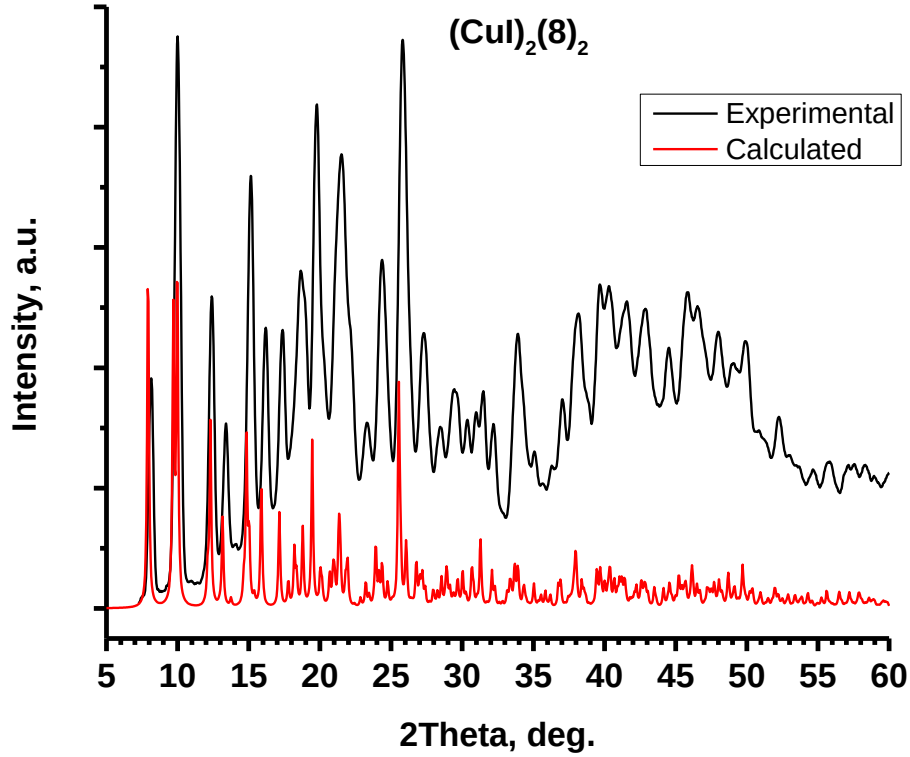

Figure S11. X-ray powder diffraction comparison of unreacted $(CuI)_2(\mathbf{3})$ (black trace), $(CuI)_2(\mathbf{3})$ stirred in 5% Py/toluene for two hours (red trace), and $(CuI)_4Py_4$ (blue trace), showing the conversion of $(CuI)_2(\mathbf{3})$ to $(CuI)_4Py_4$ on exposure to Py.

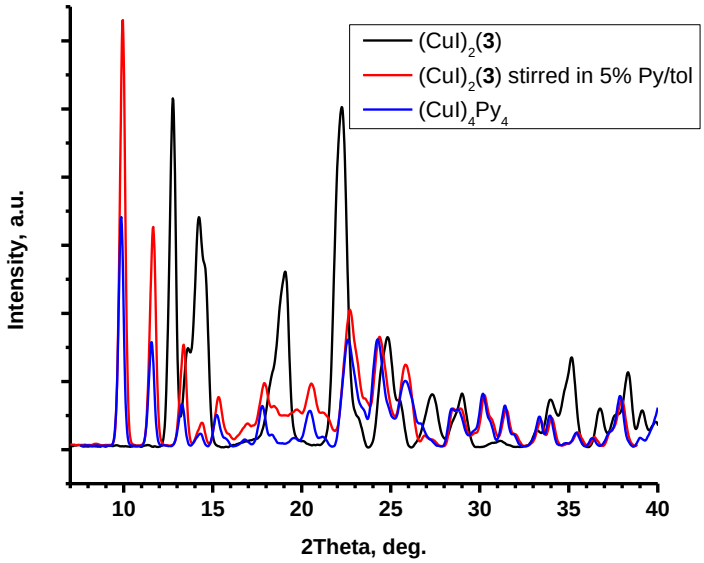

Figure S12. TGA for $(CuI)_4(\mathbf{1})_2$.

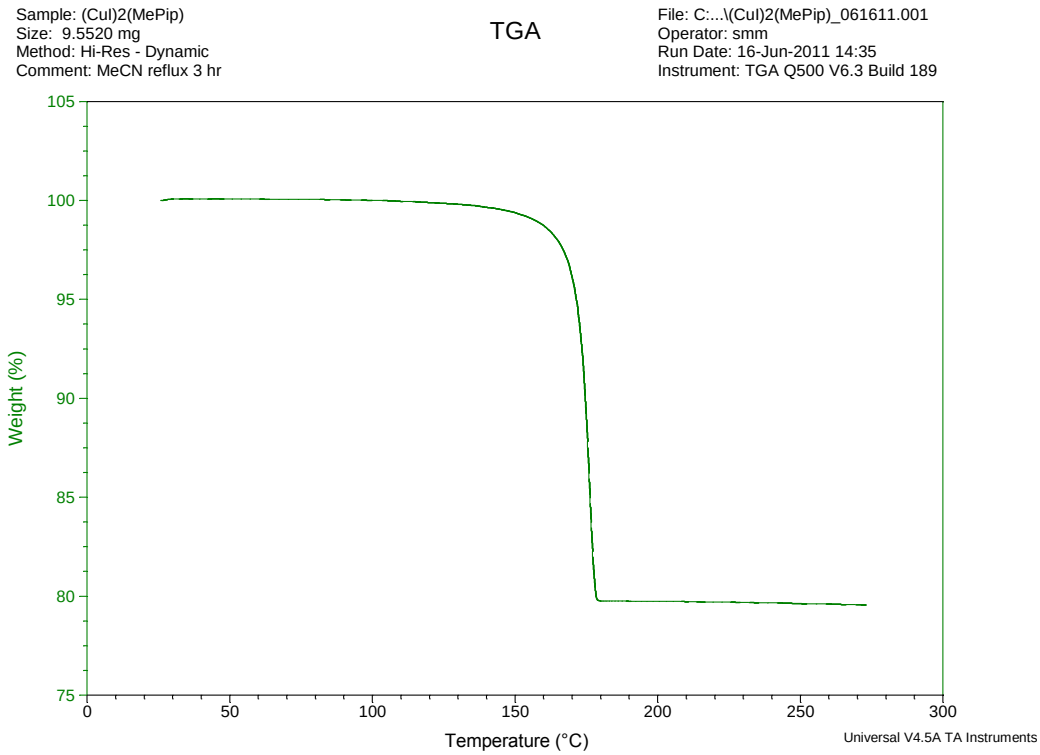

Figure S13. TGA for $(CuBr)_4(\mathbf{2})_2$.

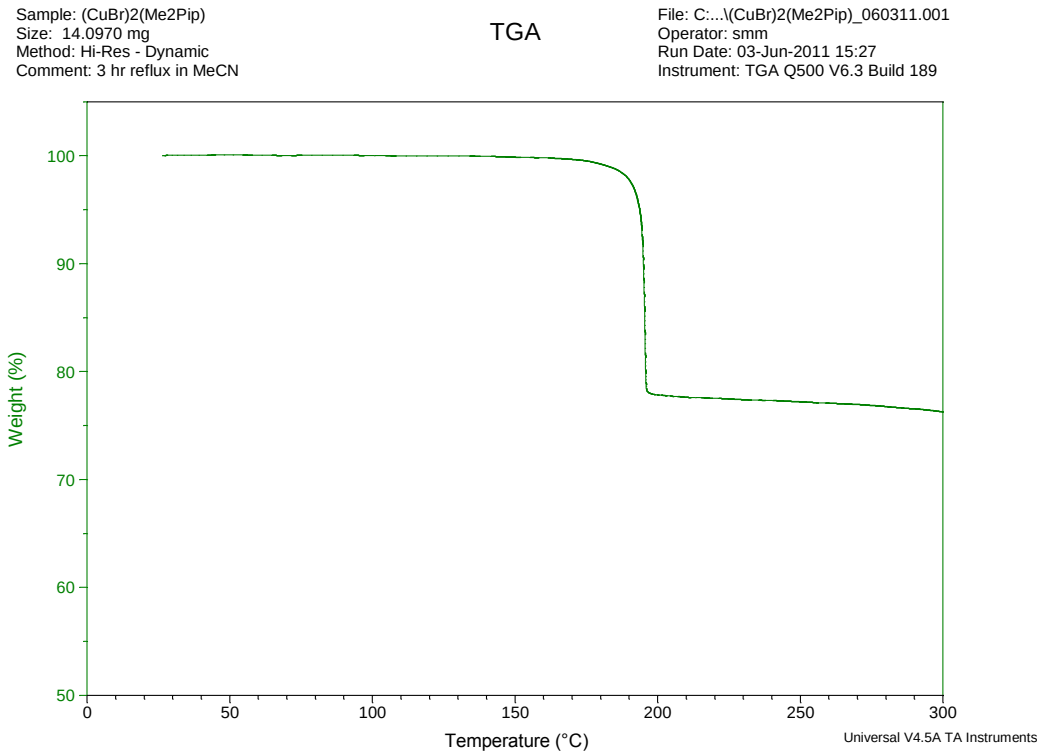

Figure S14. TGA for $(CuI)_4(\mathbf{2})_2$.

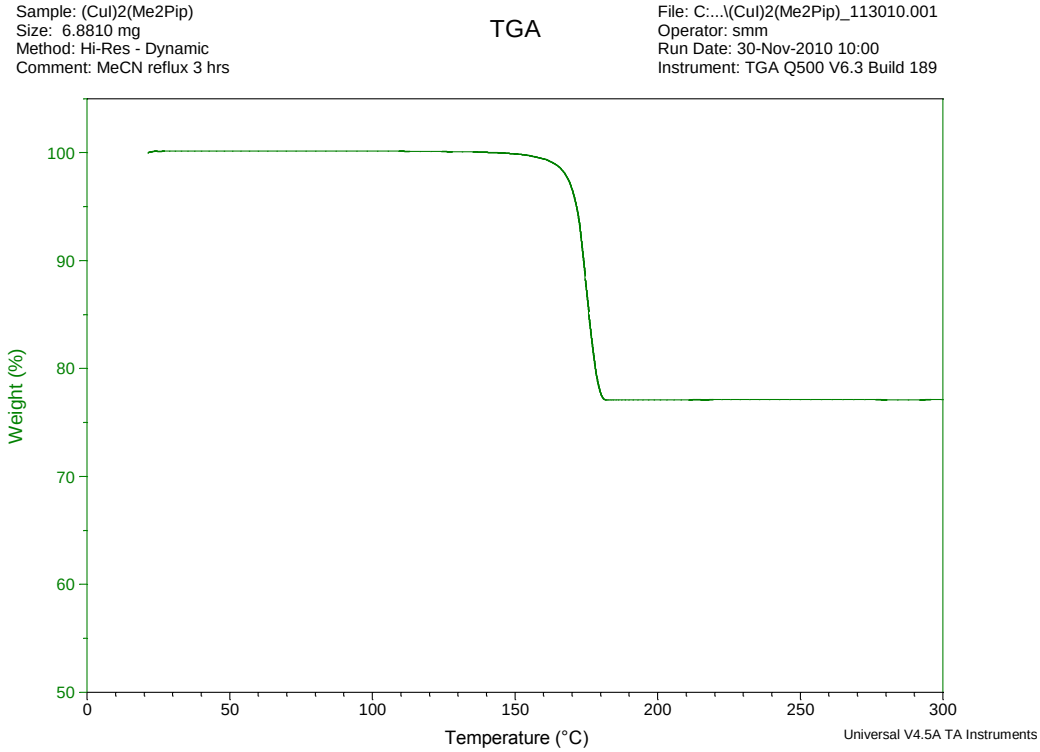

Figure S15. TGA for $(CuI)_2(\mathbf{3})$.

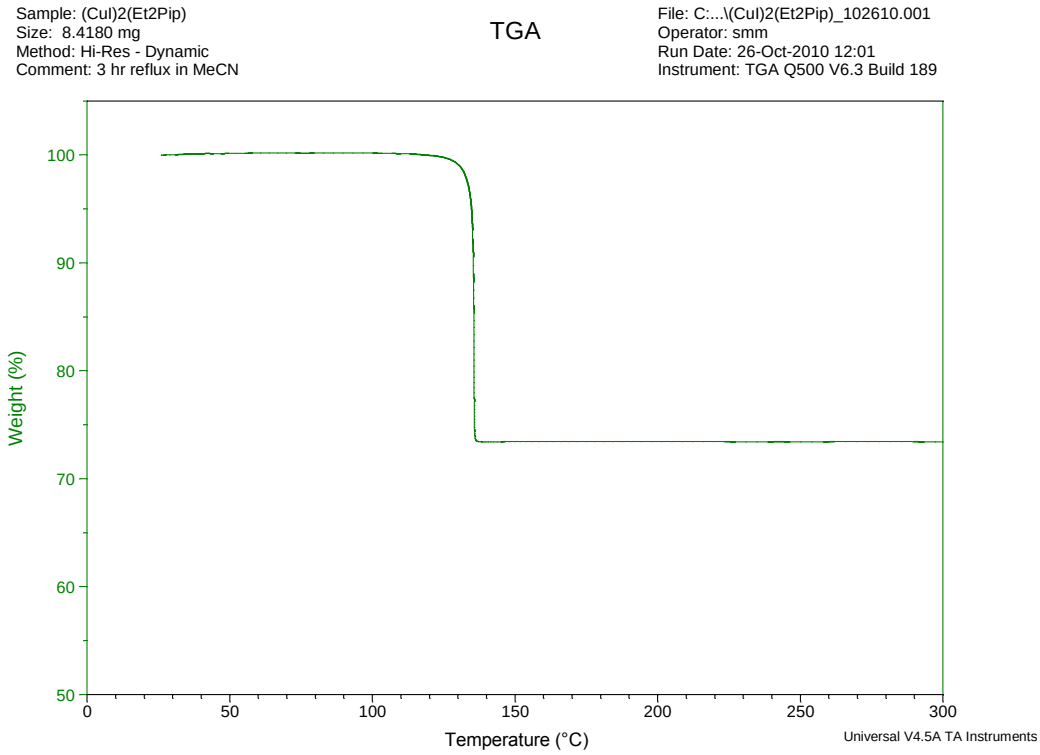

Figure S16. TGA for $(CuI)_2$(**4**).

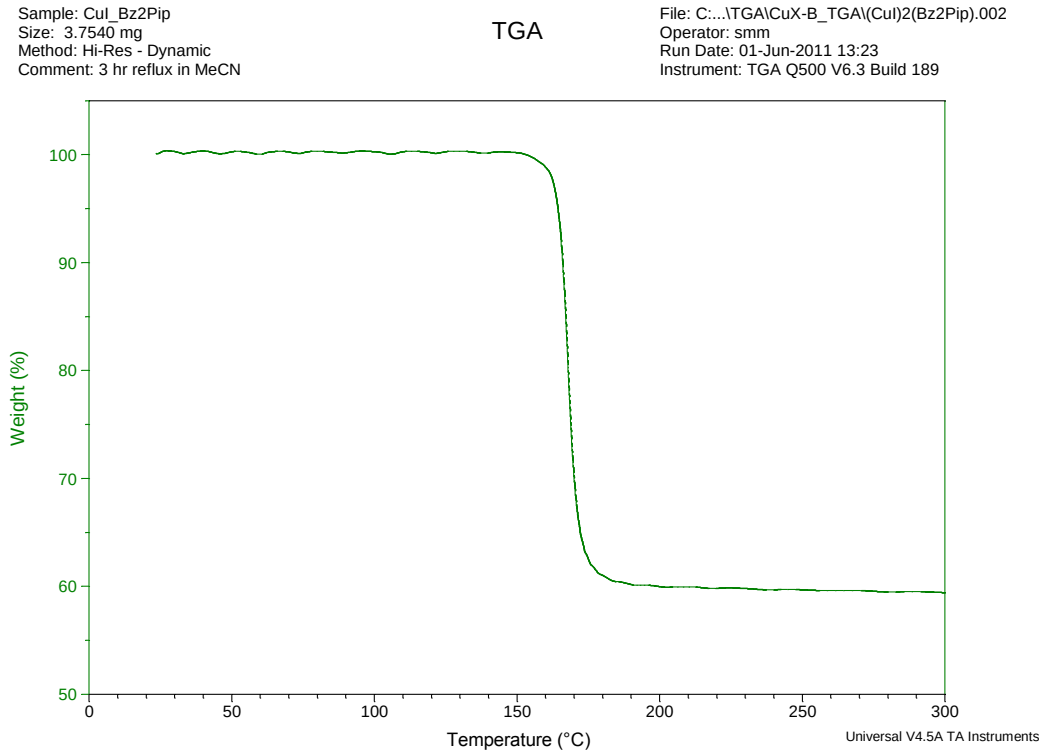

Figure S17. TGA for $(CuI)_2$(**5**).

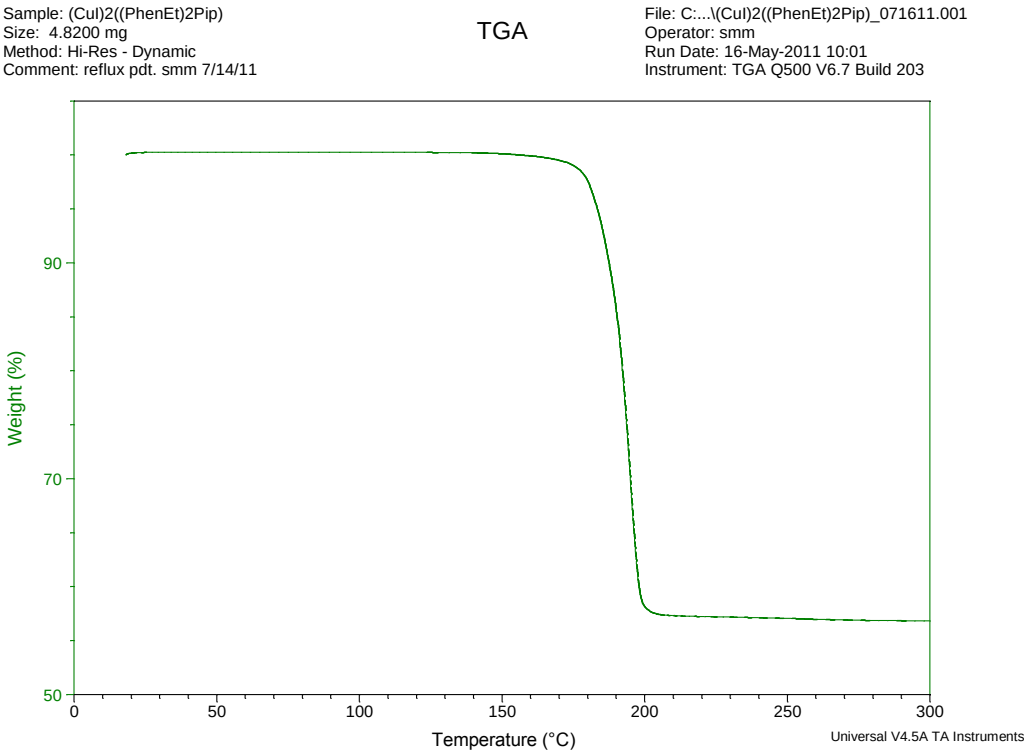

Figure S18. TGA for $(CuI)_4(\mathbf{6})_4$.

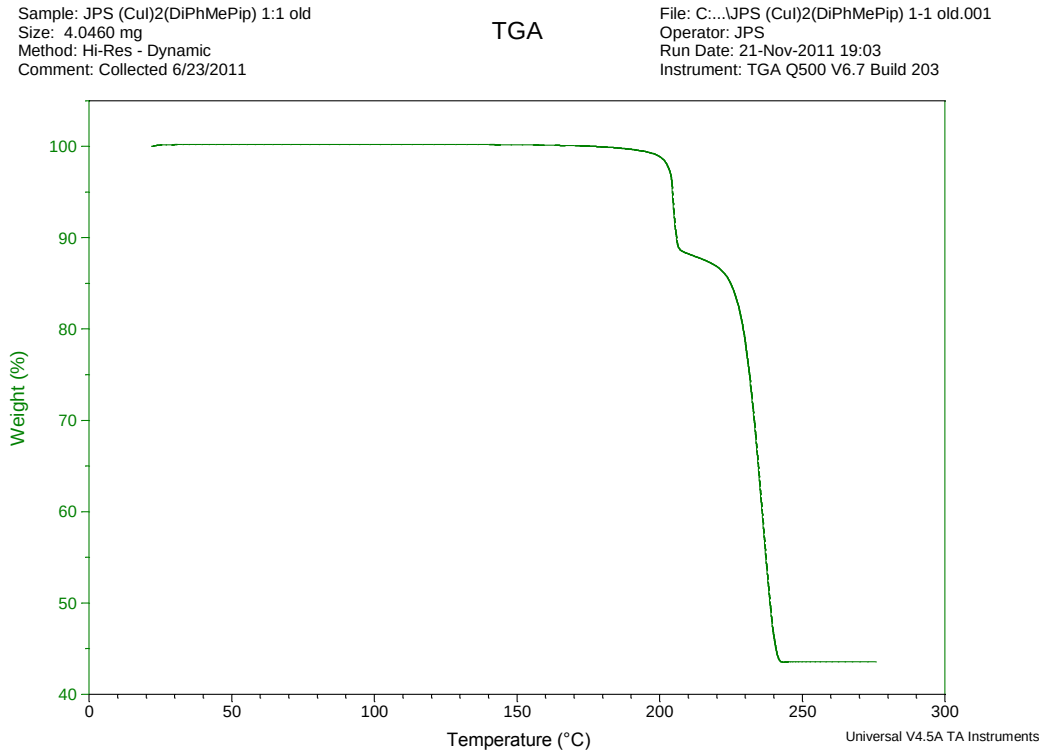

Figure S19. TGA for $(CuI)_2(\mathbf{7})$.

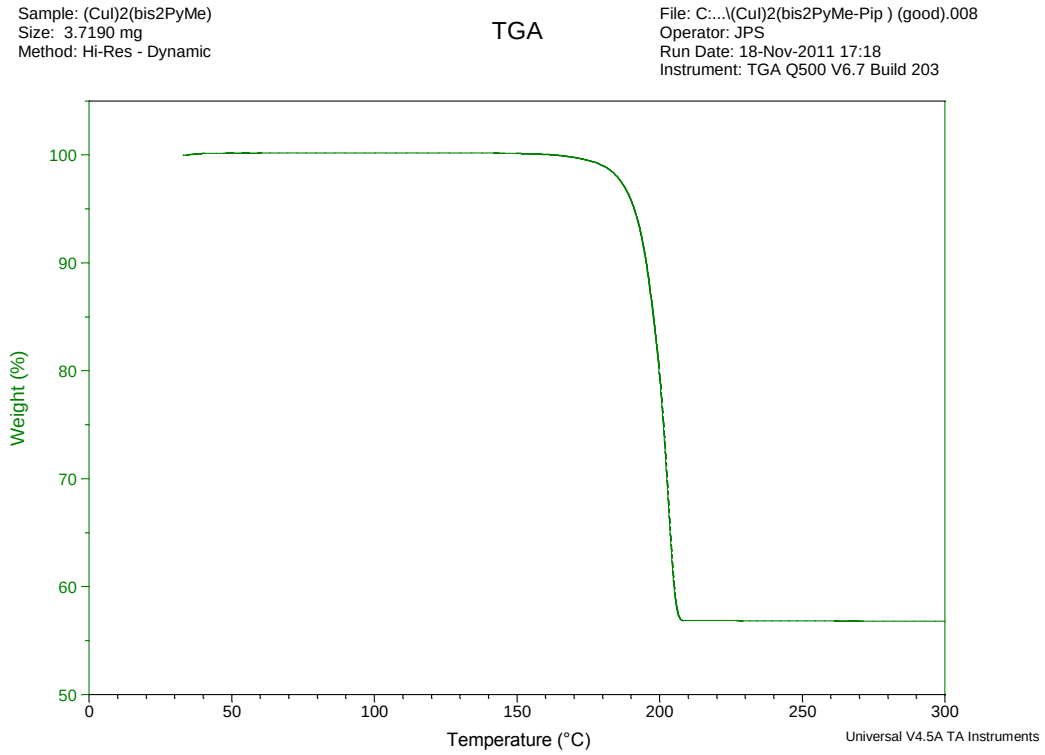

Figure S20. TGA for $(CuI)_2(\mathbf{8})_2$.

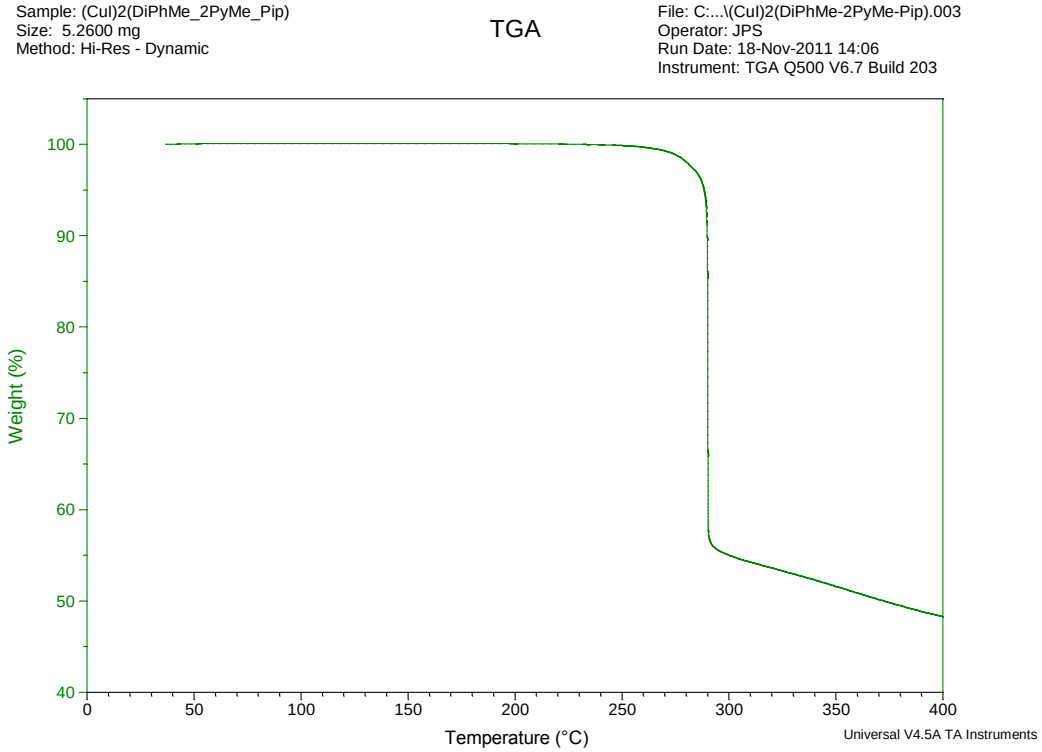

Figure S21. Luminescence spectra of $(CuI)_4(\mathbf{1})_2$ at 298 and 77 K.

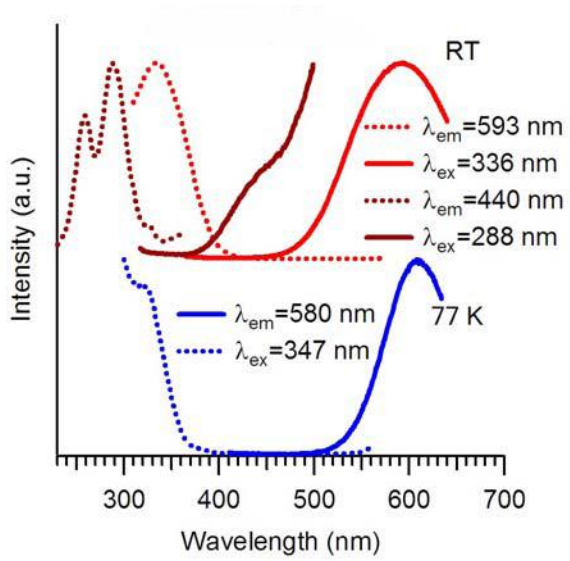

Figure S22. Luminescence spectra of $(CuBr)_4(\mathbf{2})_2$ at 298 and 77 K.

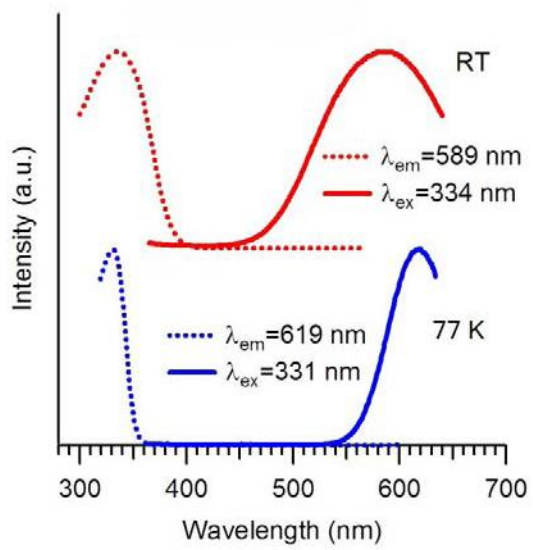

Figure S23. Luminescence spectra of $(CuI)_4(\mathbf{2})_2$ at 298 and 77 K.

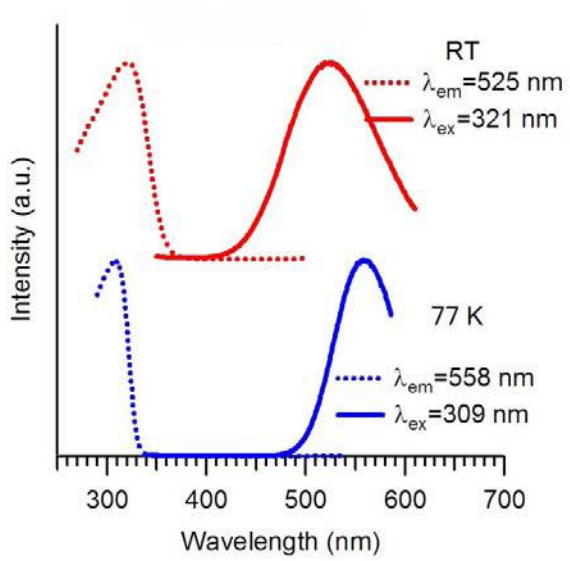

Figure S24. Luminescence spectra of $(CuI)_2(\mathbf{3})$ at 298 and 77 K.

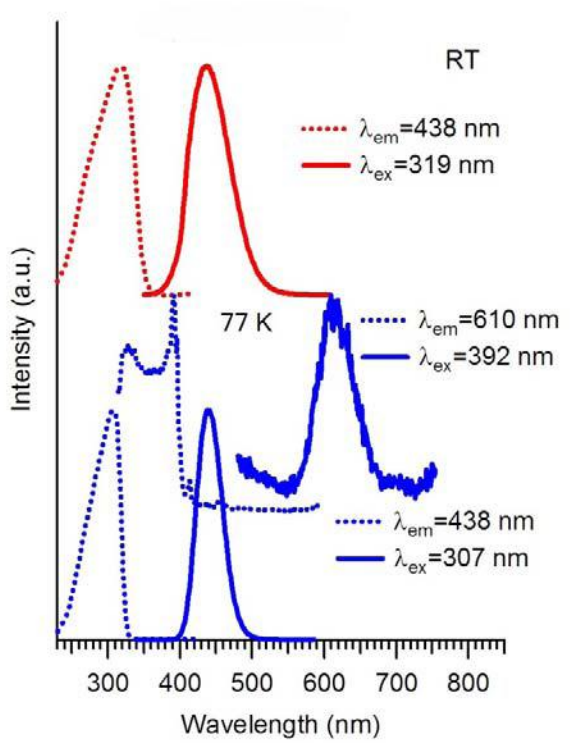

Figure S25. Luminescence spectra of $(CuI)_2$(**4**) at 77 K. (Compound lacks luminescence at 298 K.)

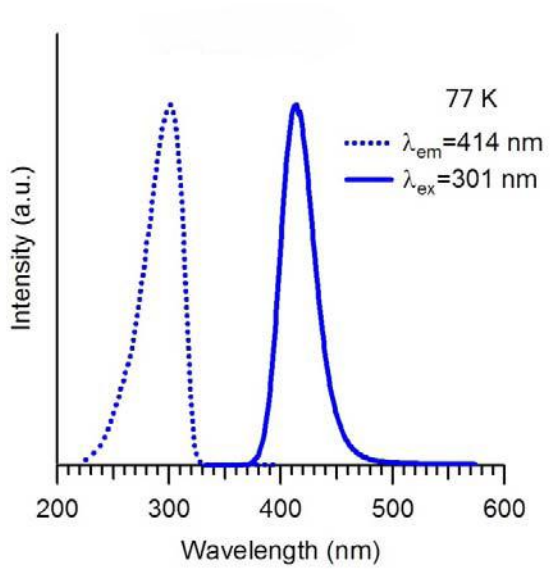

Figure S26. Luminescence spectra of $(CuI)_2$(**5**) at 298 and 77 K.

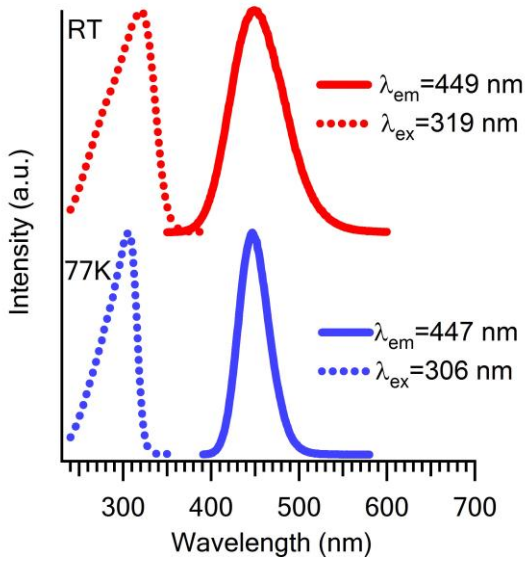

Figure S27. Luminescence spectra of $(CuI)_4(\mathbf{6})_4$ at 298 and 77 K.

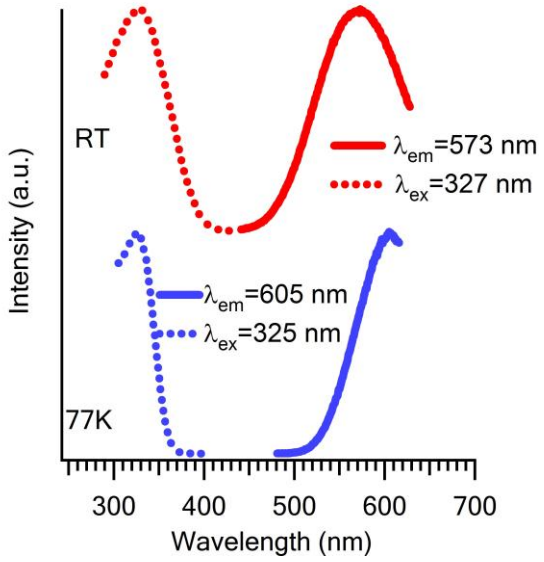

Figure S28. Luminescence spectra of $(CuI)_2(\mathbf{7})$ at 298 and 77 K.

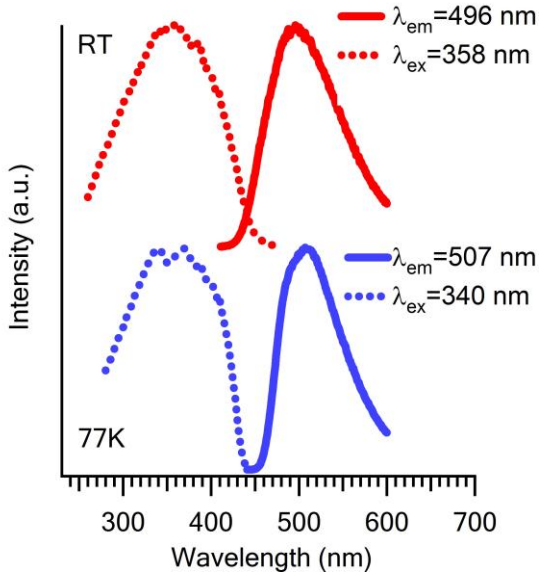

Figure S29. Luminescence spectra of $(CuI)_2(\mathbf{8})_2$ at 298 and 77 K.

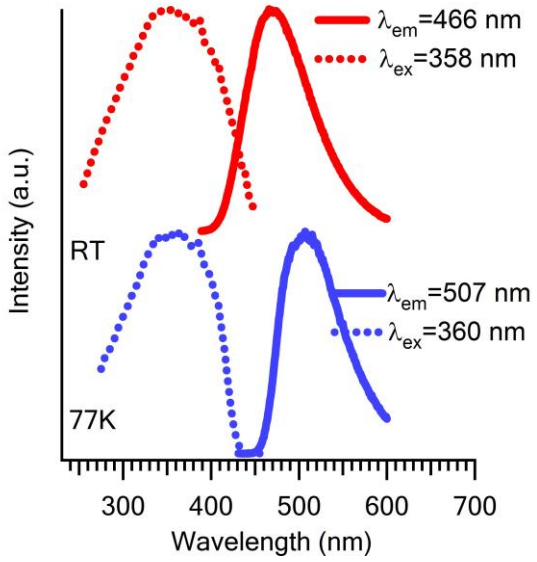

Figure S30. Plots of the cluster-based molecular orbitals of $(CuI)_2(NMe_3)_2$ (**Y**).